Biochemistry

Communication

Cite This: Biochemistry XXXX, XXX, XXX−XXX

pubs.acs.org/biochemistry

Stiffness of Cargo−Motor Linkage Tunes Myosin VI Motility and Response to Load

Rachit Shrivastava,[†,§] Ashim Rai,[‡,§] Murti Salapaka,[*,†] and Sivaraj Sivaramakrishnan[*,‡]

[†]Department of Electrical and Computer Engineering, University of Minnesota Twin Cities, Minneapolis, Minnesota 55455, United States

[‡]Department of Genetics, Cell Biology, and Development, University of Minnesota Twin Cities, Minneapolis, Minnesota 55108, United States

Supporting Information

ABSTRACT: We examine the effect of cargo−motor linkage stiffness on the mechanobiological properties of the molecular motor myosin VI. We use the programmability of DNA nanostructures to modulate cargo−motor linkage stiffness and combine it with high-precision optical trapping measurements to measure the effect of linkage stiffness on the motile properties of myosin VI. Our results reveal that a stiff cargo−motor linkage leads to shorter step sizes and load-induced anchoring of myosin VI, while a flexible linkage results in longer steps with frequent detachments from the actin filament under load. Our findings suggest a novel regulatory mechanism for tuning the dual cellular roles of the anchor and transporter ascribed to myosin VI.

Bustamante et al. describe the cell as a "clockwork" made up of multiple interconnected mechanical elements rather than a "reaction vessel", the analogy that was prevalent among biochemists more than half a century ago.[1] This emerging paradigm in cell biology emphasizes the importance of mechanical communication in cellular functions. Cellular processes such as cell adhesion, organelle transport, and migration rely on mechanical communication in macromolecular clusters. Effective force transmission in such ensembles depends on the mechanical properties of the linkage between biomolecules. In this study, we focus on the impact of linkage stiffness on the mechanical communication between groups of molecular motors driving the transport of cargo along cytoskeletal filaments.

Cytoskeletal motors link to their cellular cargoes through diverse mechanisms ranging from adaptor protein intermediates to lipid molecules that directly bind the motor.[2,3] The diversity in cargo−motor attachments translates into distinct linkage stiffness regimes in cellular membrane traffic. Both experimental[4−6] and theoretical studies[7−10] have shown that linkage stiffness alters motile properties, such as the velocity and run length of cytoskeletal motors. However, the mechanistic basis of these changes, in terms of stepping behavior and force generation, is not well understood and is the focus of this study.

To investigate the impact of linkage stiffness on the stepping behavior and force generation of individual motors in ensembles, we need experimental systems wherein the motor number and linkage stiffness can be controlled in concert with high-precision force spectroscopy techniques. We have previously demonstrated[11] that DNA origami scaffolds offer programmability of the motor number and linkage stiffness to impact motile properties. Here, we use optical trapping to measure the intersection of linkage stiffness and force sensitivity of myosin VI. We have adapted the system to couple DNA origami to micrometer-sized spherical beads that are subsequently used as probes in an optical trapping setup. Our assay provides resolution of piconewton forces on the motor coupled with measurements of motor movement with nanometer precision while varying the cargo−motor linkage stiffness.

The protocol for coupling DNA origami to beads and oligo-labeled myosin VI is shown in Figure 1A. Briefly, origami is coupled to avidin-coated beads via a biotinylated DNA strand, whereas the oligo-labeled myosin VI is linked to the bead−origami system via complementary base pairing.[12] To modulate cargo−motor linkage stiffness, the length of the oligo coupled to myosin VI is varied to achieve a stiff or flexible linkage of the motor to the cargo (Figure 1A, inset). To quantify the change in cargo−motor linkage stiffness, the motor linkage stiffness is measured through a clamping of the bead variance that occurs when a motor engages with the actin filament and exerts force (Figure 1B). The optical trap and the motor linkage can be modeled as springs attached in parallel to the bead (Figure 1C). Thus, the stiffness measured during a motor binding event is a sum of the stiffness of the trap and that of the motor linkage. The stiffness of the linkage can be estimated from the difference between the stiffness measured with the motor bound to the actin filament and the trap stiffness measured with the unbound bead. Moreover, the motor linkage is a combination of the oligo spring attaching the motor to the origami and the inherent motor spring connected in series to each other (Figure 1C, inset). Because myosin VI is common for both a stiff and a flexible linkage, the change in the linkage stiffness is essentially a function of the oligo spring stiffness. Quantification of the linkage stiffness distributions measured for a stiff versus flexible linkage is

Special Issue: Mechanical Forces in Biochemistry

Received: May 10, 2019
Revised: August 27, 2019
Published: September 11, 2019

DOI: 10.1021/acs.biochem.9b00422
Biochemistry XXXX, XXX, XXX−XXX

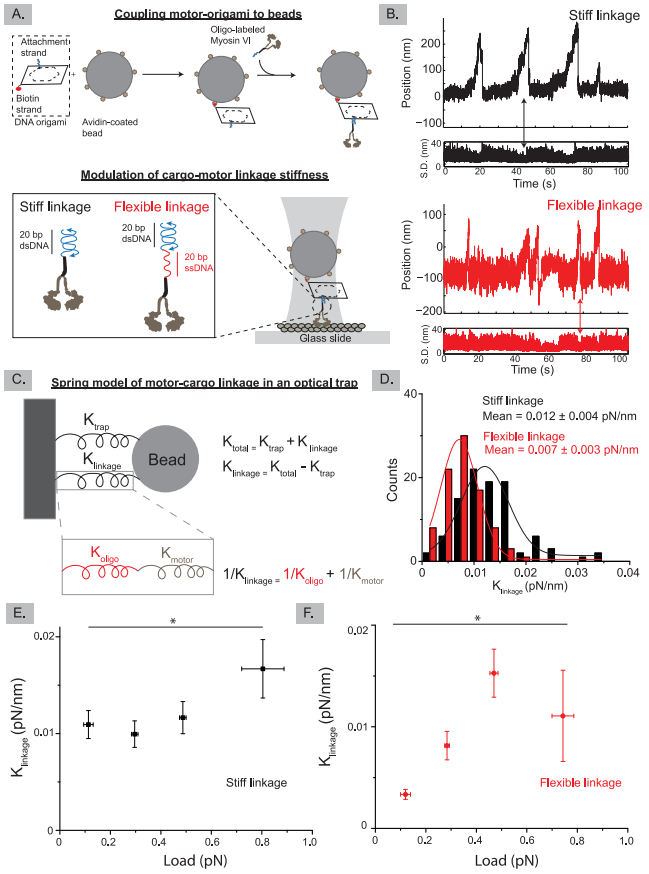

Figure 1. (A) Schematic illustrating the protocol for coupling DNA origami scaffolds and oligo-labeled myosin VI to beads for optical trapping (top) and the rationale for changing linkage stiffness via the length of the single-stranded DNA oligo coupled to myosin VI (inset, bottom). (B) Representative position vs time plots of myosin VI force generation events in an optical trap when connected via a stiff vs flexible linkage. Also shown is the standard deviation (S.D.) in position to illustrate the clamping of bead variance (double-headed arrow) that occurs when myosin VI binds to an actin filament. (C) Model of the cargo linkage and optical trap coupled to the bead as elastic springs in parallel. The inset shows the cargo linkage spring as a combination of the oligo and myosin VI spring connected in series to each other. (D) Distribution of linkage stiffness for a stiff vs flexible linkage. Both distributions have been fit to a single-peak Gaussian with R^2 values of 0.87 for a stiff linkage and 0.99 for a flexible linkage. n = 97 and 89 variance clamping events pooled from three different protein preparations of myosin VI were used for linkage stiffness calculation for the stiff and flexible linkage, respectively. A Z-test was used to estimate the statistical significance of the difference between mean stiffness at the $P < 0.001$ level. Error values are reported as the standard deviation. (E and F) Linkage stiffness plotted as a function of load for stiff and flexible linkages. Error bars are standard deviations. The number in parentheses below each data point indicates the number of events used to generate the values of that data point. Significance between the linkage stiffness at the lowest load and highest load points was estimated using a one-way analysis of variance with a post hoc Tukey's test ($P < 0.05$). The overall weighted average load experienced by a stiff linkage (0.32 pN) was found to be higher than that of a flexible linkage (0.26 pN).

shown in Figure 1D. We observe a significant decrease ($P < 0.001$) in cargo−motor linkage stiffness when myosin VI is coupled to DNA origami through a flexible oligo link (mean of 0.007 ± 0.003 pN/nm) when compared to a stiff oligo linkage (mean of 0.012 ± 0.004 pN/nm). Because the applied load could have an impact on the stiffness of the linkage, we measured changes in linkage stiffness as a function of load (Figure 1E,F). Indeed, we observed a load-dependent stiffening of the entire linkage at higher loads for both stiff and flexible linkage geometries. Given that the majority of events (~75%) occur at low loads (<0.5 pN), the use of single- and double-stranded DNA linkages to modulate stiffness is appropriate for motor ensembles under low-load conditions.

After quantifying the change in linkage stiffness using a flexible oligo link, we investigated the effect of linkage stiffness on the motility of myosin VI attached to DNA origami. The unloaded motility of a stiff versus a flexible linkage was assessed as shown in Figure 2B. The single-molecule motility

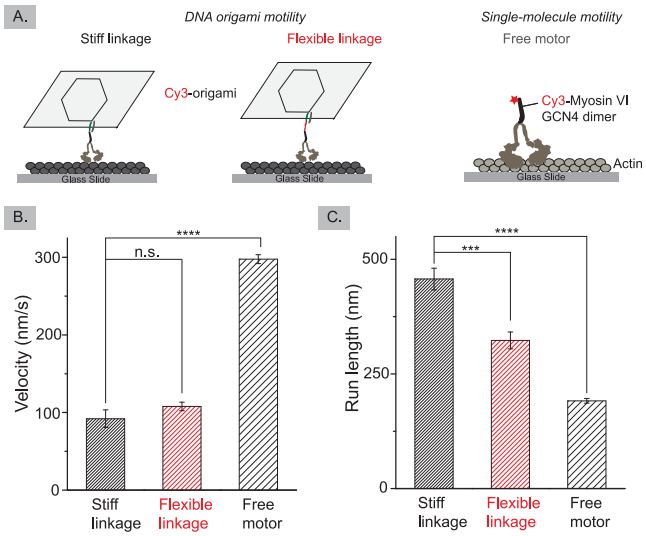

Figure 2. (A) Schematic for the motility assay when origami is attached to myosin VI via a stiff linkage (left), via a flexible linkage (middle), and without origami, i.e., free motor (right). (B) Average velocities (nanometers per second) for a stiff linkage, a flexible linkage, and a free motor case. (C) Average run lengths (nanometers) for a stiff linkage, a flexible linkage, and a free motor case. A Student's t test was used to estimate the significance of the difference between mean values of velocity and run length. N > 1000 motility events across three different protein preparations were used to obtain mean values of velocity and run length. Error values are reported as the standard error of the mean.

of myosin VI without any cargo attached (free motor) is used as a control to assess the effect of cargo binding and cargo size on motility. We observe that the velocities for myosin VI bound to DNA origami (92 ± 11 nm/s for a stiff linkage and 107 ± 5 nm/s for a flexible linkage) are lower than that for myosin VI without DNA origami (297 ± 5 nm/s). In contrast, the run lengths for myosin VI bound to DNA origami (457 ± 23 nm for a stiff linkage and 323 ± 18 nm for a flexible linkage) are higher than that of myosin VI without DNA origami (191 ± 5 nm). The physical basis of the differences observed in the motile properties of the free versus origami-bound myosin VI is unclear. Nonetheless, the velocities with flexible and stiff linkages were not found to be significantly different. In contrast, there was a significant decrease ($P < 0.001$) in run length observed with a flexible linkage (mean of 323 ± 18 nm) compared to that with a stiff linkage (mean of 457 ± 23 nm) (Figure 2C). The increase in run length with a stiff linkage could result from an effect of linkage stiffness on the load-dependent motor properties of myosin VI such as step size and

DOI: 10.1021/acs.biochem.9b00422
Biochemistry XXXX, XXX, XXX−XXX

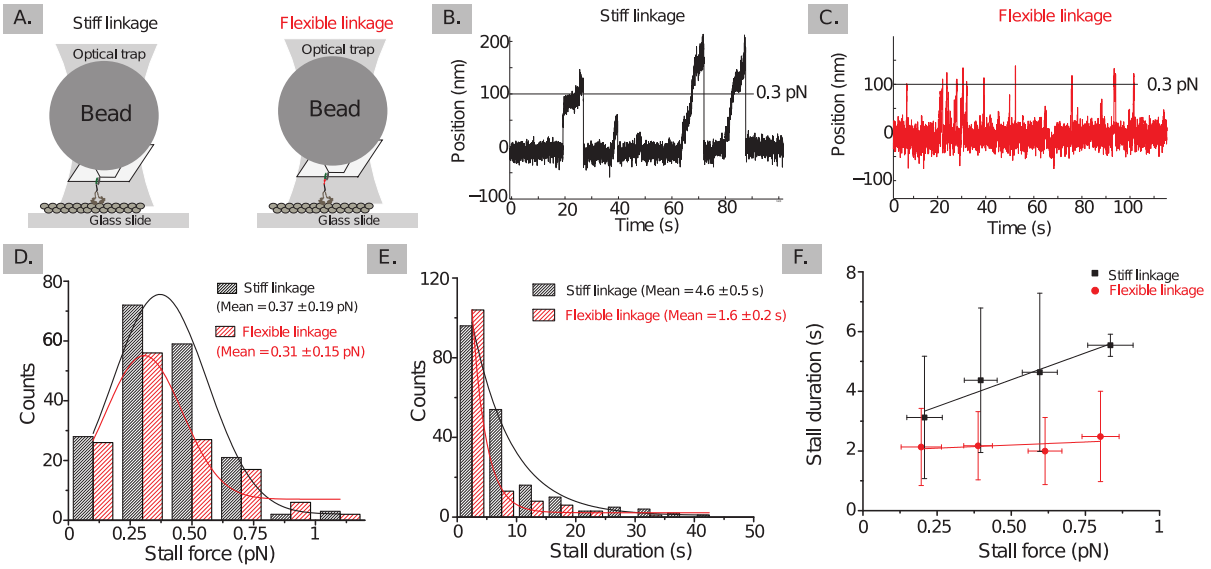

Figure 3. (A) Schematic illustrating the optical trapping geometries with stiff and flexible cargo−motor linkages for myosin VI. (B and C) Representative force generation events with stiff and flexible linkages for myosin VI, respectively. As illustrated, a stiff linkage is characterized by force generation events that last longer than flexible linkage events. (D) Distribution of stall forces for myosin VI with stiff (black) and flexible (red) cargo−motor linkages. R^2 = 0.99 and 0.87 for the Gaussian fits of stiff and flexible linkages, respectively ($P < 0.01$). (E) Stall duration distributions for stiff vs flexible linkage fit to a single-exponential decay with mean values indicated in the plot. R^2 = 0.98 and 0.99 for the single-exponential fit of stiff and flexible linkages, respectively. A flexible linkage exhibits a significantly shorter ($P < 0.001$) stall duration compared to that of a stiff linkage. (F) Correlation of stall force against stall duration as a measure of the ability of myosin VI to sustain load. For a stiff linkage, there is a linear improvement in the stall duration with an increasing stall force that does not happen for a flexible linkage of myosin VI (smaller slope). The slope of the linear fit was 3.59 s/pN for a stiff linkage and 0.41 s/pN for a flexible linkage. N = 192 and 136 force generation events pooled from three different protein preparations of myosin VI were used for stall force and stall duration calculation for the stiff and flexible linkages, respectively. Error bars are standard deviations. The Z-test was used to determine the statistical significance in differences.

detachment rate. Thus, we next measured the impact of linkage stiffness on the load-dependent motor properties of myosin VI using optical trapping (Figure 3A).

To investigate the effect of linkage stiffness on myosin VI behavior under load, we first quantified the force at which the motor stalls (stall force) and the time for which the motor is able to sustain the stall load (stall duration). A stall event is defined as the decrease in the motor velocity to <10 nm/s during a force generation event in the optical trap. The stall duration was the duration from the beginning of a stall event to the point at which the motor detached and the bead fell back to the center of the trap. The force generation profile of myosin VI in panels B and C of Figure 3 shows that myosin VI connected via a stiff linkage exhibits longer stalling events, whereas myosin VI connected via a flexible linkage displays multiple shorter stall events in a similar time window. The stalling profile of myosin VI was quantified in terms of stall force and stall duration. The stall force distributions shown in Figure 3D indicate that there is an increase ($P < 0.01$) in the stall force for myosin VI connected with a stiff linkage (mean of 0.37 ± 0.19 pN) compared to that of a flexible linkage (mean of 0.31 ± 0.15 pN). Also, the stall duration (see Figure 3E) was significantly higher ($P < 0.001$) for myosin VI connected with a stiff linkage (mean of 4.6 ± 0.5 s) than that of a flexible linkage (mean of 1.6 ± 0.2 s). Furthermore, the stall duration showed a higher rate of increase with an increasing stall force (see Figure 3F) for myosin VI when it is attached via a stiff linkage (slope of 3.59 s/pN) compared to that of myosin VI connected via a flexible linkage (slope of 0.41 s/pN). This faster increase in stall duration with an increasing load for myosin VI attached through a stiff linkage parallels the load-induced anchoring of myosin VI seen in earlier optical trap measurements.[13,14]

To understand the effect of linkage flexibility on the stepping behavior of myosin VI, we analyzed the optical trapping data to obtain the step size and time interval between the subsequent steps (dwell time) of myosin VI connected via stiff and flexible linkages to the beads (Figure 4A,B). Step size distributions (Figure 4C) reveal a significant increase ($P < 0.001$) in step size for myosin VI connected via a flexible linkage (mean of 28 ± 13 nm) compared to a stiff linkage (mean of 19 ± 10 nm). It was also observed that the dwell time between steps changed considerably with linkage stiffness (Figure 4D). The mean dwell time for myosin VI connected via a stiff linkage (mean of 0.9 ± 0.5 s) was found to be significantly higher ($P < 0.001$) than that for a flexible linkage (mean of 0.3 ± 0.1 s). Because both the step size and the dwell time are shown to be load-dependent for other processive motors,[15,16] we next measured the step size and dwell time as a function of applied load for both stiff and flexible linkages (Figure 4E−H). We observed no significant trend in step size or dwell time of myosin VI with an increasing load for both stiff and flexible linkages. It is important to note here that our measurements were performed at physiological ATP concentrations (2 mM) and the dwell time has previously been shown to be dependent on ATP concentration.[14] Therefore, the observations described herein are consistent with previous literature of myosin VI stepping where neither the step size nor the dwell time of myosin VI was observed to have a load dependence at physiological ATP concentrations and loads of <2 pN.[14]

In this study, we have investigated the impact of cargo−motor linkage stiffness on myosin VI transport. A stiff cargo−myosin VI linkage results in load-induced anchoring of myosin

DOI: 10.1021/acs.biochem.9b00422
Biochemistry XXXX, XXX, XXX−XXX

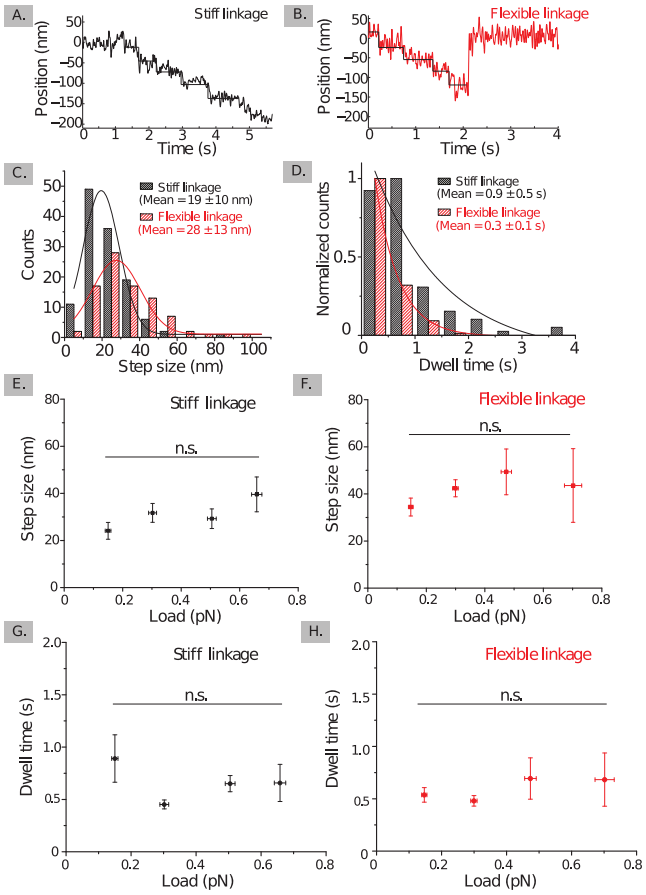

Figure 4. (A and B) Representative bead position data showing the stepping profile for myosin VI attached with stiff and a flexible linkages, respectively. (C) Distribution of step sizes of myosin VI with stiff (black) and flexible (red) cargo−motor linkages. The distributions are fit to a single-peak Gaussian with R^2 values of 0.93 and 0.88 for stiff and flexible linkages, respectively. There is an increase in the mean step size of myosin VI connected with a flexible linkage ($P < 0.001$). (D) Distribution of dwell times of myosin VI with stiff (black) and flexible (red) cargo−motor linkages. The dwell time distributions are fitted to a single exponential with R^2 values of 0.99 and 0.96 for stiff and flexible linkages, respectively. Myosin VI attached with a stiff linkage shows a significantly higher mean dwell time ($P < 0.001$) compared to that of a flexible linkage. $N = 124$ and 89 stepping events pooled from three different protein preparations of myosin VI were used for step size and dwell time calculation for the stiff and flexible linkages, respectively. (E and F) Step size as a function of load for stiff and flexible linkages, respectively. Error values are standard deviations. Significance between the linkage stiffness at the lowest load and highest load points was estimated using a one-way analysis of variance (ANOVA) with a post hoc Tukey's test. (G and H) Dwell time between steps as a function of load for stiff and flexible linkages, respectively. Error bars are standard deviations. Significance between the linkage stiffness at the lowest load and highest load points was estimated using a one-way ANOVA with a post hoc Tukey's test. The *Z*-test was used for statistical significance in differences. Error bars are standard deviations.

VI characterized by a longer stall duration, a longer dwell time between steps, and shorter step sizes. In contrast, a flexible cargo−myosin VI linkage leads to frequent detachments under load, resulting in shorter stall durations and dwell times between steps. Interestingly, however, a flexible linkage leads to longer step sizes for myosin VI presumably through extension of the effective myosin VI lever arm.[17] Theoretical modeling of motor transport has previously predicted an inverse relationship between the dwell time and load-dependent rate of detachment of the motor from the filament.[18] Also, Kunwar et al. have shown through Monte Carlo simulations of motor transport that a decreased linkage stiffness leads to impaired collective motor function due to stretching of the linkage and higher detachment rates.[19] Our results provide experimental validation for such a role of linkage stiffness in regulating the load-dependent behavior of the motor suggested by the aforementioned theoretical models. A flexible linkage provides greater Brownian diffusion of the two heads relative to the cargo scaffold [$\Delta x = \sqrt{K_b T}/\sqrt{K_{linkage}}$ (Figure 4C)], stochastically enabling a larger step size. In contrast, the flexible linkage yields smaller resistive loads (Figure 1E,F) for the same distance traveled by the myosin dimer. Consequently, the load-induced anchoring phenomenon that has been well-documented for myosin VI[14,20] is not engaged as frequently in the presence of a flexible linkage.

Myosin VI has been ascribed dual functionality as a transporter and a tether function inside the cell.[21] It acts as a transporter to processively move organelles such as endosomes and secretory vesicles, whereas it functions as a molecular tether to maintain the structure of stereocilia in inner ear hair cells.[22] Myosin VI was shown to display load-induced anchoring at higher loads in optical trapping experiments,[13,14] which likely forms the mechanistic basis for its dual functions. However, previous studies did not explore a role for linkage stiffness in the load-induced anchoring behavior of myosin VI. The results presented here highlight the cargo−myosin VI linkage stiffness as an additional layer of regulation for load-induced anchoring of myosin VI whereby both transporter and anchor roles can be tuned by the mechanical properties of the motor−cargo attachment.

In conclusion, the methodology described in this study combines DNA origami with optical trapping and opens up avenues of studying the effect of cargo−motor linkage stiffness on motor transport. Enabled by the methodology, our results reveal that the mechanical properties of the cargo−motor linkage play a key role in regulating the cellular context-dependent function of myosin VI.

■ ASSOCIATED CONTENT

Supporting Information

The Supporting Information is available free of charge on the ACS Publications website at DOI: 10.1021/acs.biochem.9b00422.

Details of materials, methods, experimental setup, and software used to analyze the data (PDF)

Accession Codes

Unconventional myosin VI from *Homo sapiens*, UniProt Accession ID Q9UM54.

■ AUTHOR INFORMATION

Corresponding Authors

*E-mail: murti@umn.edu.
*E-mail: sivaraj@umn.edu.

ORCID

Sivaraj Sivaramakrishnan: 0000-0002-9541-6994

Author Contributions

§R.S. and A.R. contributed equally to this work.

DOI: 10.1021/acs.biochem.9b00422
Biochemistry XXXX, XXX, XXX−XXX

Funding

This work was supported by the National Institutes of Health (1R35GM126940-01 to S.S.) and the National Science Foundation (CNS 1544721 to M.S.).

Notes

The authors declare no competing financial interest.

REFERENCES

(1) Bustamante, C., Chemla, Y. R., Forde, N. R., and Izhaky, D. (2004) Mechanical Processes in Biochemistry. *Annu. Rev. Biochem. 73*, 705−748.

(2) Pathak, D., and Mallik, R. (2017) Lipid - Motor Interactions: Soap Opera or Symphony? *Curr. Opin. Cell Biol. 44*, 79−85.

(3) Akhmanova, A., and Hammer, J. A. I. (2010) Linking molecular motors to membrane cargo. *Curr. Opin. Cell Biol. 22*, 479−487.

(4) Berger, F., Keller, C., Klumpp, S., and Lipowsky, R. (2015) External forces influence the elastic coupling effects during cargo transport by molecular motors. *Phys. Rev. E 91*, 022701.

(5) Hughes, J., Hancock, W. O., and Fricks, J. (2012) Kinesins with extended neck linkers: a chemomechanical model for variable-length stepping. *Bull. Math. Biol. 74*, 1066−1097.

(6) Hariadi, R. F., Sommese, R. F., Adhikari, A. S., Taylor, R. E., Sutton, S., Spudich, J. A., and Sivaramakrishnan, S. (2015) Mechanical coordination in motor ensembles revealed using engineered artificial myosin filaments. *Nat. Nanotechnol. 10*, 696−700.

(7) Fricks, J., Wang, H., and Elston, T. C. (2006) A numerical algorithm for investigating the role of the motor-cargo linkage in molecular motor-driven transport. *J. Theor. Biol. 239*, 33−48.

(8) Materassi, D., Roychowdhury, S., Hays, T., and Salapaka, M. (2013) An exact approach for studying cargo transport by an ensemble of molecular motors. *BMC Biophys. 6*, 14.

(9) Bhaban, S., Materassi, D., Li, M., Hays, T., and Salapaka, M. (2016) Interrogating Emergent Transport Properties for Molecular Motor Ensembles: A Semi- analytical Approach. *PLoS Comput. Biol. 12*, e1005152.

(10) Bhat, D., and Gopalakrishnan, M. (2016) Transport of organelles by elastically coupled motor proteins. *Eur. Phys. J. E: Soft Matter Biol. Phys. 39*, 71.

(11) Hariadi, R. F., Sommese, R., and Sivaramakrishnan, S. (2015) Tuning myosin-driven sorting on cellular actin networks. *eLife 4*, e05472.

(12) Hariadi, R. F., Cale, M., and Sivaramakrishnan, S. (2014) Myosin lever arm directs collective motion on cellular actin network. *Proc. Natl. Acad. Sci. U. S. A. 111*, 4091−4096.

(13) Chuan, P., Spudich, J. A., and Dunn, A. R. (2011) Robust mechanosensing and tension generation by myosin VI. *J. Mol. Biol. 405*, 105−112.

(14) Altman, D., Sweeney, H. L., and Spudich, J. A. (2004) The mechanism of myosin VI translocation and its load-induced anchoring. *Cell 116*, 737−749.

(15) Mallik, R., Carter, B. C., Lex, S. A., King, S. J., and Gross, S. P. (2004) Cytoplasmic dynein functions as a gear in response to load. *Nature 427*, 649.

(16) Clemen, A. E.-M., Vilfan, M., Jaud, J., Zhang, J., Bärmann, M., and Rief, M. (2005) Force-dependent stepping kinetics of myosin-V. *Biophys. J. 88*, 4402−4410.

(17) Yu, C., Lou, J., Wu, J., Pan, L., Feng, W., and Zhang, M. (2012) Membrane-induced lever arm expansion allows myosin VI to walk with large and variable step sizes. *J. Biol. Chem. 287*, 35021−35035.

(18) Bouzat, S., and Falo, F. (2010) The influence of direct motor-motor interaction in models for cargo transport by a single team of motors. *Phys. Biol. 7*, 046009.

(19) Kunwar, A., Vershinin, M., Xu, J., and Gross, S. P. (2008) Stepping, Strain Gating, and an Unexpected Force-Velocity Curve for Multiple-Motor-Based Transport. *Curr. Biol. 18*, 1173−1183.

(20) Sweeney, H. L., Park, H., Zong, A. B., Yang, Z., Selvin, P. R., and Rosenfeld, S. S. (2007) How myosin VI coordinates its heads during processive movement. *EMBO J. 26*, 2682−2692.

(21) Lu, Q., Li, J., and Zhang, M. (2014) Cargo recognition and cargo-mediated regulation of unconventional myosins. *Acc. Chem. Res. 47*, 3061−3070.

(22) Self, T., Sobe, T., Copeland, N. G., Jenkins, N. A., Avraham, K. B., and Steel, K. P. (1999) Role of myosin VI in the differentiation of cochlear hair cells. *Dev. Biol. 214*, 331−341.

DOI: 10.1021/acs.biochem.9b00422
Biochemistry XXXX, XXX, XXX−XXX